Computational Simulations of the Lateral-Photovoltage-Scanning-Method

IOP Conf. Series: Materials Science and Engineering **355** (2018) 012019 doi:10.1088/1757-899X/355/1/012019

Computational Simulations of the Lateral-Photovoltage-Scanning-Method

S Kayser, A Lüdge and K Böttcher
Leibniz Institute for Crystal Growth, Max-Born-Straße 2, D-12489 Berlin, Germany

e-Mail: Stefan.Kayser@ikz-berlin.de

Abstract. The major task for the **L**ateral-**P**hotovoltage-**S**canning-Method is to detect doping striations and the shape of the solid-liquid-interface of an indirect semiconductor crystal. This method is sensitive to the gradient of the charge carrier density. Attempting to simulate the signal generation of the **LPS**-Method, we are using a three dimensional Finite Volume approach for solving the van Roosbroeck equations with COMSOL Multiphysics in a silicon sample. We show that the simulated LPS-voltage is directly proportional to the gradient of a given doping distribution, which is also the case for the measured LPS-voltage.

1. Introduction

Among the methods for crystal growth from the melt there are several techniques where the growing crystal is in permanent rotation inside of an inhomogeneous temperature field. For the Floating Zone technique this is, above all, caused by the gap in the heating coil. Consequently, each point of the melt sees a periodically changing temperature field leading to corresponding convection patterns. The additionally fluctuating doping concentration at the crystal-melt-interface leads to 3-dimensional concentration profiles roughly in form of a spiral staircase. The geometric shape of the 3D profiles follows the shape of the crystal-melt-interface. Making a cut through the crystal in growth direction results in a crystal surface with a periodical concentration pattern that reveals the growth history of the crystal-melt-interface, which again represents a finger print of the individual single crystal. The **L**ateral-**P**hotovoltage-**S**canning-Method (**LPS**) is known to be the method of choice for detecting these doping inhomogeneities in grown semiconductors, such as silicon [1], germanium [2] and silicon-germanium [3].

A first important question is, which local resolution can be achieved with respect to the mean free path of the charge carriers. In order to answer this question, a simulation of this measurement technique is established using a Finite Volume approach.

2. Experimental

Figure 1 shows the measurement setup of the LPS-Method. Here, a modulated laser ($f = 1$ kHz, square-wave) is focused ($\emptyset = (10 - 30)$ µm) on a semiconductor sample and generates excess photo carriers. If a dopant gradient exists at that observation point, the generated electrons and holes will drift in different directions due to the inner electric field [4]. Hence, a local dipole will be generated temporarily. This leads to a potential difference between the ohmic rim contacts (U_{LPS}), which can be amplified and detected with respect to the modulation frequency.

The measurement is carried out by changing the focal point of the laser and detecting $U_{\mathrm{LPS}}\,(x,y)$. This signal is known to be proportional to the gradient of the dopant distribution: $U_{\mathrm{LPS}}\,(x,y) \propto \nabla_{\mathrm{x}}\, N_{\mathrm{D}}^{+}(x,y)$ [1].

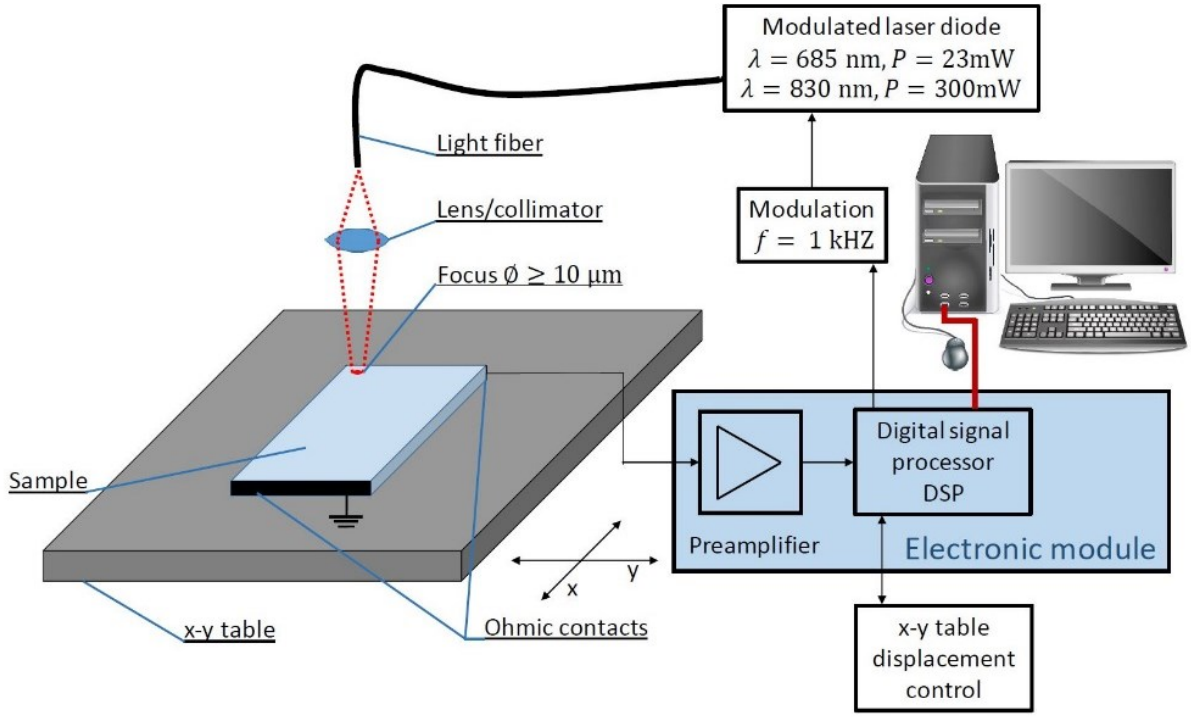

Figure 1. Scheme of the LPS-measurement setup. A modulated laser generates electrons/holes locally. If there is a gradient on the doping distribution at the observation point, a voltage difference will be detectable at the ohmic rim contacts. This voltage is amplified with respect to the modulation frequency.

3. Computational Simulation

3.1. Equation System

The fundamental equation system for the charge carrier flow and the electrostatic potential in a semiconductor structure is named after van Roosbroeck [5]. This system consists of three nonlinear coupled partial differential equations for the three physical variables, the electrostatic potential $\boldsymbol{\Psi}(\boldsymbol{r})$, the densities of electrons $n(\boldsymbol{r})$ and of holes $p(\boldsymbol{r})$. The potential and the charge carrier densities obey the Poisson equation of the electric field, which is in detail:

$$-\nabla \cdot \left(\epsilon_0 \epsilon_{\mathrm{r}}\, \nabla \boldsymbol{\Psi}(\boldsymbol{r})\right) = \mathrm{q}(p(\boldsymbol{r}) - n(\boldsymbol{r}) + N_{\mathrm{D}}^{+} - N_{\mathrm{A}}^{-}), \tag{1}$$

with the vacuum permittivity ϵ_0 and relative permittivity ϵ_{r}, the elementary charge q, and the densities of ionized donors and acceptors N_{D}^{+} and N_{A}^{-}.

The continuity equations for electrons (2) and holes (3) consider both the generation rate $G(\boldsymbol{r})$ and the recombination rate $R(\boldsymbol{r})$:

$$\frac{\partial n}{\partial t} - \frac{1}{\mathrm{q}} \nabla \cdot \boldsymbol{j}_{\mathrm{n}}(\boldsymbol{r}) = G(\boldsymbol{r}) - R(\boldsymbol{r}), \tag{2}$$

$$\frac{\partial p}{\partial t} + \frac{1}{\mathrm{q}} \nabla \cdot \boldsymbol{j}_{\mathrm{p}}(\boldsymbol{r}) = G(\boldsymbol{r}) - R(\boldsymbol{r}). \tag{3}$$

In the van Roosbroeck equation system (1), (2) and (3) the current densities are modelled as a sum of drift and diffusion currents:

$$-\boldsymbol{j}_{\mathrm{n}}(\boldsymbol{r}) = \mathrm{q}[\mu_{\mathrm{n}} n(\boldsymbol{r}) \nabla \boldsymbol{\Psi}(\boldsymbol{r}) - D_{\mathrm{n}} \nabla n(\boldsymbol{r})],$$
$$-\boldsymbol{j}_{\mathrm{p}}(\boldsymbol{r}) = \mathrm{q}\left[\mu_{\mathrm{p}} p(\boldsymbol{r}) \nabla \boldsymbol{\Psi}(\boldsymbol{r}) + D_{\mathrm{p}} \nabla p(\boldsymbol{r})\right].$$

3.2. Specifications

For the energy distribution of electrons and holes we choose the Fermi-Dirac statistics, hence, the diffusion coefficients of electrons D_{n} and holes D_{p}, are related to the mobilities of electrons μ_{n} and holes μ_{p} by the generalized Einstein relation

$$\text{electrons:} \quad \frac{D_{\mathrm{n}}}{\mu_{\mathrm{n}}} = \frac{\mathrm{k_B} T}{\mathrm{q}} g\left(\frac{n}{N_{\mathrm{c}}}\right),$$
$$\text{holes:} \quad \frac{D_{\mathrm{p}}}{\mu_{\mathrm{p}}} = \frac{\mathrm{k_B} T}{\mathrm{q}} g\left(\frac{p}{N_{\mathrm{v}}}\right),$$

where k_{B} is the Boltzmann constant, T is the temperature, and N_{c} and N_{v} are the conduction and valence band density of states, resp., g is a nonlinear factor ($g > 1$), which considers the Fermi-Dirac statistics.

The generation of electrons and holes are determined by the energy of the incoming laser beam. The laser is moved by a velocity v_{L} along the x-direction focussed on the surface of the silicon sample during time t. The laser beam intensity profile is assumed to have a Gaussian distribution, and the laser spot size is defined according to the traditional definition at which the diameter is taken transverse to the beam axis at which the intensity profile falls to $1/\mathrm{e}^2 \;\widehat{=}\; 13.5\,\%$ of the intensity peak [6]. In terms of the Gaussian distribution, the standard deviation of the laser intensity in x and y-direction at the surface of the silicon sample is just a quarter of the $1/\mathrm{e}^2$-diameter, and we assume them to be identical $\sigma_{\mathrm{x}} = \sigma_{\mathrm{y}} = d_{1/\mathrm{e}^2}/4$ [6].

When denoting the peak power of the laser by P_0 and the photon energy by $E_{\mathrm{ph}}\,[\mathrm{Ws}] = \mathrm{hc}/\lambda$ with λ as wavelength of the laser beam, h as Planck constant, and c as light velocity, then the total photon flow rate is $I_{\mathrm{tot}} = P_0/E_{\mathrm{ph}} = P_0\,\lambda/\mathrm{hc}$, which still needs to be shaped by the two-dimensional Gaussian distribution which itself includes the movement of the laser beam in x-direction. Finally the photon flux is

$$I_{\mathrm{F}}(x,y,t)\left[\frac{1}{\mathrm{m^2 s}}\right] = I_{\mathrm{tot}} \frac{1}{2\pi\sigma_{\mathrm{x}}\sigma_{\mathrm{y}}} \exp\left[-\frac{(x - x_0 - v_{\mathrm{L}} t)^2}{2\sigma_{\mathrm{x}}^2} - \frac{(y - y_0)^2}{2\sigma_{\mathrm{y}}^2}\right]$$

The photon flux impinging at the surface penetrates into the depth of the crystal sample which is the (negative) z-direction. The penetration depth is practically limited due to the absorption coefficient $A_{\mathrm{c}}\,[1/\mathrm{m}]$. Nevertheless, there is a three-dimensional generation rate of electrons and holes:

$$G(x,y,z,t)\left[\frac{1}{\mathrm{m^3 s}}\right] = A_{\mathrm{c}} \exp[-A_{\mathrm{c}}|z|]\; I_{\mathrm{F}}(x,y,t).$$

We are denoting that the simulations are done for room temperature, neglecting the heating by the laser.

The recombination rate on the right side of equation (2) and (3) consists of the most common processes: the direct recombination R_{Direct}, the Shockley-Read-Hall recombination R_{SRH}, and the Auger recombination R_{Auger}:

$$R(x,y,z,t) = R_{\mathrm{Direct}} + R_{\mathrm{SRH}} + R_{\mathrm{Auger}}.$$

Every recombination process is implemented in COMSOL Multiphysics and is realized by supplying material dependent recombination rates.

Figure 2 illustrates that all boundaries Γ_{N} of the platelet are electrically isolated except the end-faces of the silicon sample: one (Γ_1) of the two is set to the equilibrium potential, the other is established as an ideal ohmic contact with current connection ($i_{\Gamma_2}(t)$) to an external circuit. In order to detect the voltage change at the end-faces of the platelet, the experimental setup includes an internal resistance R in an electrical circuit model.

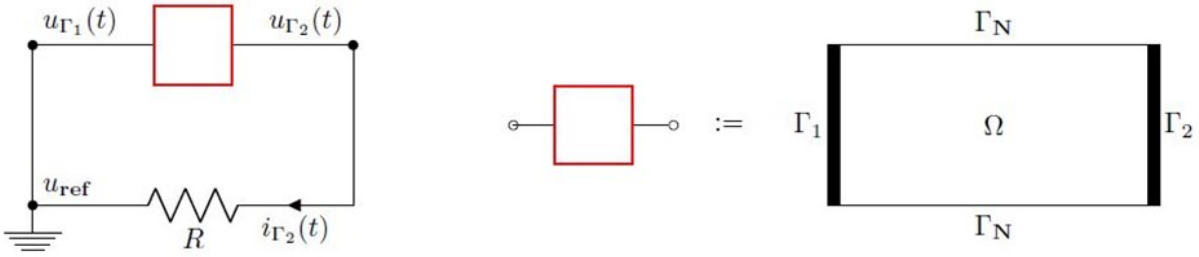

Figure 2. Scheme of the modelled electrical circuit and the boundary conditions of the sample Ω.

3.3. Numerical Procedure

The computational model was solved by using the software COMSOL Multiphysics V. 5.2a [7]. We use the "semiconductor module" and the "electrical circuit module".

The variables of the semiconductor part are the electric potential, the electron concentration and the hole concentration. The electric circuit part computes voltages and currents. Due to the thickness of the silicon platelet we have a 3-dimensional geometry which is meshed by a mapped grid ($x-y$-plane) that is swept in z-direction.

We held to the standard options of COMSOL for semiconductor problems: the Finite Volume Method is the numerical procedure, the numerical stability is reached by applying the Scharfetter-Gummel scheme [8].

4. Results and Discussion

The crystal is assumed to have a doping profile of boron or phosphorus, caused by segregation $N_{\mathrm{D,seg}}$, which is characterized by a macroscopic gradient along the sample length and local fluctuations. This profile is modelled by the formula:

$$N_{\mathrm{D}}^{+} = N_{\mathrm{D,seg}} + N_{\mathrm{D,fluct}} = N_{\mathrm{D,0}}\left(1 + \frac{a}{L}x + b \cdot f(x,y,z)\right), \tag{4}$$

where $N_{\mathrm{D,0}}$ is the background level of the dopant concentration, $L = 2.4$ mm is the sample length, x the length coordinate, a a control parameter for setting the macroscopic gradient of the dopant profile. The fluctuations of the doping concentration caused by temperature inhomogeneities are assumed as sinusoidal and suppressed by the prefactor $b = 10^{-5}$. The constant macroscopic gradient of the dopant profile, i.e. the linear behaviour of the profile, is assumed due to the small sample length: indeed there is a rather exponential distribution due to the segregation of, e.g., phosphorus in the melt during crystal growth.

The computation of the simulated LPS-voltage is shown in figure 3 for different values of the control parameter a in the time intervall $t \in [0.3\ 0.4]$ s. During this, the focus of the laser ($\sigma = 7.5$ µm) has moved between $x \in [0.9\ 1.2]$ mm (see upper axis). After a short loading phase of electrons and holes (where generation and recombination are not in equilibrium; see the vertical line at $t = 0.3$ s after the switch on) the computation yields a nearly constant LPS-voltage for each a-value when time runs.

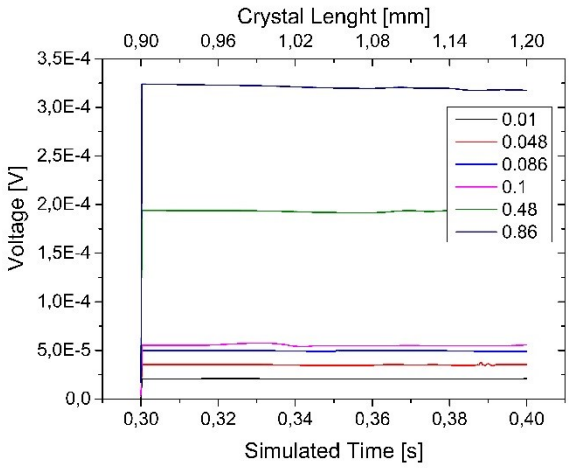

Figure 3. Result of time-dependent simulations of the LPS-voltage relative to the parameter a. Sample size: $th = 2\mu m$, $wd = 500\mu m$.

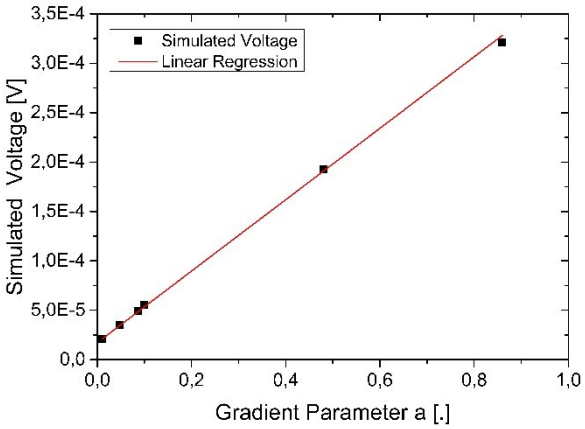

Figure 4. Dependency of the simulated LPS-voltages on the gradient parameter a.

Figure 4 shows the proportionality of the simulated LPS-voltage on the gradient of the dopant profile a. Additionally, Figure 4 reveals an offset of the LPS-voltage for $U_{\mathrm{Sim}}|_{a=0}$. In that case only the sin-shaped dopant fluctuations remain, hence, the offset cannot have physical reasons.

Therefore, we analysed, whether the offset depends on the model itself. We started to increase the sample width (from $wd = 150$ µm) and thickness (from $th = 2$ µm). As shown in figure 5, enlarging the sample width by a factor of 10 reduces the offset roughly by the same factor, however, the reduction of the offset is not a linear function of the sample width.

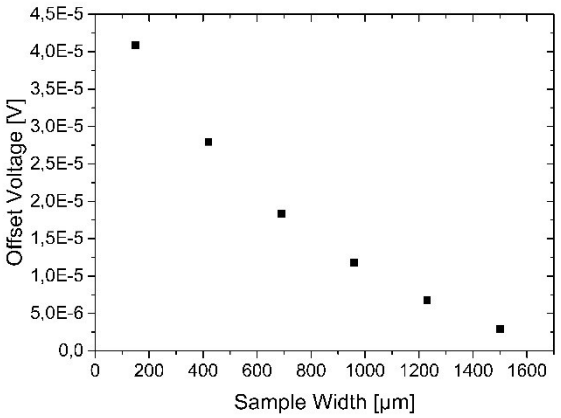

Figure 5. Behaviour of the offset with respect to the width of the simulated sample.

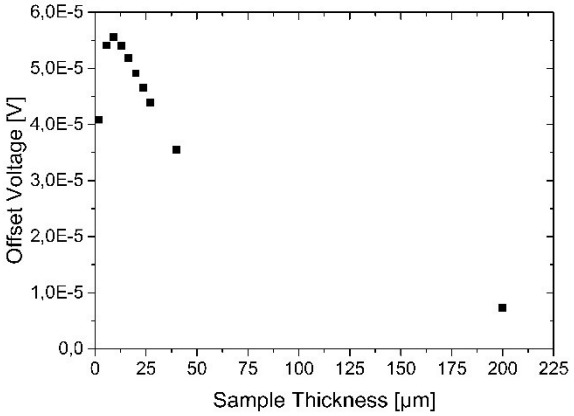

Figure 6. Dependency of the offset from the sample thickness. After an increase related to the penetration depth of the laser, a decreasing trend is visible.

The effect of the thickness on the offset is more complicated, see figure 6: as long as the sample thickness is below the penetration depth ($pd = 15.4$ µm), thickness enlargement increases the total number of charge carriers and the offset voltage is rising. But even before reaching the saturation of the total number of charge carriers, which may be reached at $th \approx 3pd$ (95 %), the offset decreases. The enlargement from the rather small thickness ($th = 2$µm) with maximum offset ($th_{\mathrm{max,off}} \approx 9\mu m$) to a thickness of $th = 200$ µm reduces the offset by a factor of eight. Because of $th \gg pd$, the non-reflected energy of the laser is absorbed (99.9998 %) by the semiconductor and transmission is highly suppressed. Combining the increased thickness and width of the sample, the offset is reduced tremendously and, thus, is negligible.

The linear dependency of the simulated LPS-voltage on a and the knowledge that $U_{\mathrm{LPS}} \propto \nabla_{\mathrm{x}} N_{\mathrm{D}}^{+}$ [1] allows the following relation:

$$U_{\mathrm{Sim}} \propto a \propto \nabla_{\mathrm{x}} N_{\mathrm{D}}^{+} \propto U_{\mathrm{LPS}}.$$

This shows that the simulated LPS-voltage corresponds to the measured LPS-voltage.

5. Conclusions and Outlook

For large enough samples ($wd \geq 1500$ µm, $th \geq 200$ µm) we have shown that the simulated LPS-voltage is directly proportional to the measured voltage $U_{\mathrm{Sim}} \propto U_{\mathrm{LPS}}$ as expected from experimental results. Simulation costs are high for such large samples, but can be reduced using symmetry assumptions (e.g. $N_{\mathrm{D}}^{+}(x,y) = N_{\mathrm{D}}^{+}(x,-y)$).

Now the local resolution can be calculated and related to the LPS-measurement method. Also, for a given mean charge carrier density (e.g. via Hall-measurements) it is possible to calculate the absolute value of the doping concentration by integration of the LPS-measurement results. This could lead to a resistivity profile with an improved local resolution compared to 4-point-measurement systems. We estimate the order of magnitude of the resolution to be hundred microns.

References

[1] Lüdge A, Riemann H, 1997 Doping Inhomogeneities in Silicon Crystals Detected by the Lateral Photovoltage Scanning (LPS) Method., *Inst. Phys. Conf.* Ser. No **160,** 145ff

[2] Wünscher M, Lüdge A, Riemann H, 2011 Crucible-free pulling of germanium crystals., *Journal of Crystal Growth,* Vol. **318**, pp 1039-1042

[3] Abrosimov N V, Lüdge A, Riemann H, Schröder W, 2002 Lateral photovoltage scanning (LPS) method for the visualization of the solid-liquid interface of Si_{1-x} Ge_x single crystals, *Journal of Crystal Growth*, Vol. **237-239**, pp 356-360

[4] Schurig T, Matz H, Drung D, Lüdge A, Riemann H, 1997 Nondestructive Wafer Inspection utilizing SQUIDs, *Inst. Phys. Conf. Ser*. No **160**, 149ff

[5] van Roosbroeck W, 1950 Theory of the flow of electrons and holes in germanium and other semiconductors, *Bell Syst. Tech. J*., Vol. **29**, pp 560-607

[6] Marshall G F, Stutz G E (Eds.), 2012 Handbook of Optical and Laser Scanning, *CRC Press*, Boca Raton

[7] COMSOL Multiphysics: Semiconductor Module, Users Guide V. 5.2a, 2016, *COMSOL AB*

[8] Scharfetter D L, Gummel H K, 1969 Large signal analysis of a silicon Read diode, *IEEE Trans. Electron. Dev*., Vol. **16**, 6477